Available online at www.sciencedirect.com
ScienceDirect
Journal of Nuclear Materials 372 (2008) 340–349
journal of nuclear materials
www.elsevier.com/locate/jnucmat

Characteristics of $Gd_xM_yO_z$ (M = Ti, Zr or Al) as a burnable absorber

Han Soo Kim *, Chang Yong Joung, Byung Ho Lee, Si Hyung Kim, Dong Seong Sohn

Korea Atomic Energy Research Institute, 150 Deokjindong, Yuseong, Daejeon 305-353, Republic of Korea

Received 18 December 2006; accepted 12 March 2007

Abstract

A heterogeneous type burnable absorber needs a diluent material to adjust its gadolinium concentration. TiO_2, ZrO_2 or Al_2O_3 was added to Gd_2O_3, separately and $Gd_xM_yO_z$ (M = Ti, Zr or Al) pellets were fabricated by a powder process. Pellets with a single Gd_2TiO_5 or $Gd_2Ti_2O_7$ were fabricated and their phases were confirmed by XRD. Thermal properties of the $Gd_xM_yO_z$ were measured and their thermal conductivities were determined. The thermal expansion was largest in $Gd_2Ti_2O_7$, and it decreased with a gadolinium concentration increase. $GdAlO_3$ had the highest thermal conductivity, next were the $Gd_xTi_yO_z$ phases in a reverse order of the gadolinium concentration increase. The selected candidate pellets of $Gd_xTi_yO_z$ were irradiated in the HANARO reactor, and post-irradiation examinations of the pellets were carried out in a hot cell. The examination results indicate that the thermal properties of the BP pellets should be considered to ensure an in-reactor integrity.

PACS: 67.80.Gb

1. Introduction

In order to increase nuclear fuel burn-up and to compensate for the reactivity loss due to fuel depletion and fission product buildup during service, the fuel assemblies loaded at the beginning of a reactor cycle should have a certain amount of excess reactivity. This excess reactivity in turn needs to be controlled, and an effective control method is to use a BP (burnable poison) absorber. There are two poisoning modes in the application of a BP, a homogeneous mode and a heterogeneous mode. The homogeneous poisoning mode has the advantage of an even power distribution, when compared with the heterogeneous one. But the homogeneous mode requires that most of the fuel pellets contain a certain amount of a BP absorber to secure the absorption worth [1–3]. The absorber material contained in a fuel degrades not only the sinterability of the fuel oxide but also the fuel properties including the thermal conductivity of a fuel pellet. The heterogeneous poisoning mode satisfies the requirements from a nuclear standpoint and the BP absorber does not degrade the thermo-mechanical properties of the fuel.

Gadolinium oxide has some preferable properties as a BP absorber for a heterogeneous mode because of the presence of ^{155}Gd and ^{157}Gd, which are more effective, when compared with the other lanthanides. BP pellets for the heterogeneous mode are fabricated by a powder process by using a mixture of Gd_2O_3 with a diluent additive [4–6]. The BP pellets are loaded into a cladding tube and welded at both ends to make a BP rod. The BP rods are positioned among the fuel rods in the assembly to compensate for the excess reactivity and to flatten the power distribution. The BP pellets must satisfy the necessary gadolinium concentration and material properties as required. The diluents, which are used for the adjustment of the gadolinium concentration in the BP pellet, form solid solutions with Gd_2O_3 during a sintering process, so they affect the material properties of a pellet [5,7–10].

* Corresponding author.
E-mail address: hskim4@kaeri.re.kr (H.S. Kim).

0022-3115/$ - see front matter © 2007 Elsevier B.V. All rights reserved.
doi:10.1016/j.jnucmat.2007.03.266

TiO_2, ZrO_2 and Al_2O_3 were used as diluent additives in this study. Each of the diluents was mixed with Gd_2O_3 and BP pellets in the form of $Gd_xM_yO_z$ (M = Ti, Zr or Al) were fabricated by different milling methods and sintering programs. This study tried to develop the fabrication processes for $Gd_xM_yO_z$ pellets and to analyze the thermal-material properties of the sintered pellets. Microstructures and phase structures of the BP pellets were compared with each other. Thermal properties of the pellets were measured and their thermal conductivities were derived to clarify the effects of different gadolinium concentrations and kinds of diluents. $Gd_xTi_yO_z$ pellets were irradiated in the HANARO (high-flux advanced neutron application reactor)[1] located in Korea Atomic Energy Research Institute. Visual and microstructural examinations of the irradiated pellets were carried out in a hot cell.

2. Experimental procedure

2.1. Fabrication and characterization of $Gd_xM_yO_z$ pellet

Gd_2O_3, TiO_2, ZrO_2 and Al_2O_3 powders were used as raw materials, which had more than a 99.9% purity and less than 2000 ppm of rare earth impurities. Gd_2O_3 and each of the diluent powders were weighed and mixed well in a tubular mixer. The powder mixtures were milled by three different methods: dry milling (DM) by using a planetary mill for 1 h at 300 rpm; wet milling (WM) by using a planetary mill with ethanol and zirconia balls as a milling media for 5 h at 300 rpm; attrition milling (AM) by using a continuous dry type attrition mill [11] at 150 rpm. Each of the powder mixtures was pressed into green pellets with three different diameters of 4.17 mm, 5.94 mm and 13.76 mm. Some green pellets were sintered by using a thermo-mechanical analyzer (TMA SETARAM) at 1773 K under an argon atmosphere to monitor their densification processes during a heat cycle. Based on the densification processes, sintering programs were determined by considering the milling methods, the kinds of diluents and the compositions of the green pellets. The green pellets were sintered according to the selected sintering program in air. Every batch number was identified with its composition, milling method and sintering process as shown in Table 1.

Sintered densities were measured by the immersion method. Microstructures and phase structures of the pellets with different compositions were analyzed by a ceramography and XRD (X-ray diffraction) method. The XRD analysis was performed by using a monochromatic Cu Kα radiation ($\lambda = 0.154056$ nm) on an X-ray diffractometer (MXP3A-HF, MacScience). Diffraction peaks and their intensities were estimated by using a peak-fit program of Matchmaker.

[1] Open-tank-in-pool type research reactor with the thermal power of 30 MW.

2.2. Thermal property measurements

Thermal expansions of the $Gd_xM_yO_z$ pellets were measured by using the TMA equipment. Longitudinal displacements of the pellets were monitored from room temperature to 1773 K with a heating rate of 5 K/min in an argon gas atmosphere.

$Gd_xM_yO_z$ disk specimens were prepared for the measurements of specific heat capacity (5 mm in diameter and 2 mm in thickness) and for the measurement of thermal diffusivity (10 mm in diameter and 1.5 mm in thickness). The heat capacity was measured by using DSC (differential scanning calorimeter, Netzsch 404C Pegasus) at an interval of 50 K from room temperature to 1273 K with a heating rate of 10 K/min in a nitrogen gas atmosphere. Thermal diffusivity measurements were made by means of a laser flash apparatus, SINKU-RIKO (TC-7000 VH/L). All the measurements were carried out in a vacuum at a pressure of less than 4×10^{-4} Pa. The temperature measurement of the back of the sample was conducted by using an In–Sb infrared sensor. For a consistent absorption of heating energy on the samples, the front and the back of a sample were covered with a thin graphite layer. The results were calculated by using a half time of the maximum temperature increase on the back of the sample for the thermal diffusivity.

2.3. Irradiation test and in-pile analysis

$Gd_xTi_yO_z$ pellets sampled from GT2d and GT4 were ground by using a precision centerless grinder into a diameter of 3.500 ± 0.001 mm. Fig. 1 shows a sectioned drawing and the assemblies of an irradiation capsule. Four pellets from the GT2d and GT4 were loaded into a sample tube, which was assembled with the other parts into a capsule, and an end plug was sealed by laser welding in helium. The capsule was assembled into a fuel test rig. The irradiation tests were performed for 254 EFPD (effective full power days) in the HANARO research reactor. After the irradiation, post-irradiation examinations (PIE) were performed in a hot cell. Visuals and dimensions of the irradiated pellets were checked by using a periscope and micrometers. Microstructures were observed for the radial sections of the pellets.

3. Results and discussion

3.1. Sinterabilities of the green pellets

Densification processes of the green pellets are useful to determine their sintering programs. The shrinkage curves of the Gd_2O_3 + diluent (diluent = TiO_2, ZrO_2 or Al_2O_3) are shown in Fig. 2. The shrinkage curves were characterized by the milling methods, the kinds, and the compositions of the diluents. Breakpoints were observed in the shrinkage curves, in the beginning for $Gd_2O_3 + TiO_2$ and in the middle for $Gd_2O_3 + Al_2O_3$. It is known that a break-

Table 1
Batch identifications and their fabrication processes

Batch no.	Compositions (mol.%)				Milling	Sintering program	Density (g/cm^3)	Remarks[a]
	Gd_2O_3	TiO_2	ZrO_2	Al_2O_3				
GT1d	50.0	50.0	–	–	DM	1873 K, 4 h	6.56	*E*, K_{th}, *X*
GT1w	50.0	50.0	–	–	WM	1923 K, 12 h	6.47	*M*, *E*
GT2d	45.5	54.5	–	–	AM	1873 K, 4 h	6.22	K_{th}, *X*, I_{rr}
GT2w	45.5	54.5	–	–	WM	1923 K, 12 h	6.17	*M*, *E*
GT3	33.3	66.7	–	–	WM	1923 K, 12 h	6.12	*X*, *E*
GT4	15.8	84.2	–	–	AM	1723 K, 4 h	5.32	*M*, *X*, K_{th} I_{rr}
GZ	48.5	–	51.5	–	WM	1923 K, 4 h	7.00	*M*, *X*, *E*, K_{th},
GA	52.8	–	–	47.2	DM	1973 K, 4 h	6.64	*X*, *E*, K_{th},

[a] *M*: microstructure, *E*: thermal expansion, K_{th}: thermal conductivity, *X*: XRD, and I_{rr}: irradiation/PIE.

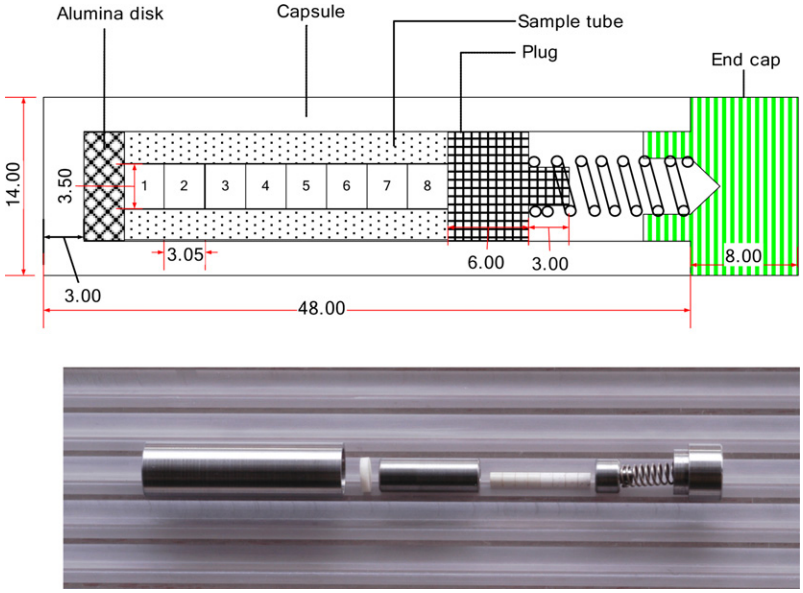

Fig. 1. Cross-section and assemblies of irradiation capsule.

point has a relation to any thermal processes such as the formation of a solid solution and/or a structural change. In the case of $Gd_2O_3 + ZrO_2$, a breakpoint was not observed in the curve. The relative ionic radius and oxygen parameter govern the formation and the stability of a solid solution in a binary oxide system. In the $Gd_2O_3 + ZrO_2$ system, Gd^{3+} and Zr^{4+} are similar in size and form a highly disordered phase as the cations occupy the same six- and eight-fold sites so that the volume change for the formation of a solid solution is negligible [9]. However, a highly ordered phase forms in the $Gd_2O_3 + TiO_2$ system because of the large difference in the ionic radii of the Gd^{3+} and the Ti^{4+} [9]. The existence of the breakpoints is due to the size difference between the cations in the binary oxide system.

Both $Gd_2O_3 + 50.0$ mol.% TiO_2 and $Gd_2O_3 + 54.5$ mol.% TiO_2 started shrinking at around 1470 K. The densification process proceeded at a maximum speed at around 1710 K and continued, even at a holding temperature of 1773 K. Both compositions of the green pellets showed a similar densification behavior, but the total shrinkages after the same heat cycle were different with regard to the compositions and milling methods. The green pellet of $Gd_2O_3 + 72.8$ mol.% TiO_2 started a shrinking process at around 1320 K and the process was saturated at around 1720 K, before arriving at the set temperature of 1773 K. The densification behavior of the $Gd_2O_3 + 72.8$ mol.% TiO_2 was distinctly different from those for the other compositions of $Gd_2O_3 + TiO_2$. Sintering temperatures need to increase with a decreasing x in $Gd_2O_3 + x$ mol.% TiO_2 to obtain homogeneous solid solutions. The phase diagram [12] shows that a eutectic reaction occurs at 1818 K, when the x is more than 66.7 mol. The green pellets with $x > 66.7$ in $Gd_2O_3 + x$ mol.% TiO_2 might be sintered below 1773 K to avoid a melt down or bonding of the pellets to a ceramic support. The densification process of $Gd_2O_3 + ZrO_2$ is similar to that of $Gd_2O_3 + TiO_2$, except for the appearance of breakpoints, during the heat cycle. $Gd_2O_3 + ZrO_2$ can be sintered at the same conditions as those of $Gd_2O_3 + TiO_2$. For the green pellets of $Gd_2O_3 + Al_2O_3$, the breakpoints appeared above 1580 K. The formation of a solid solution between Gd_2O_3 and Al_2O_3 occurred after the densification

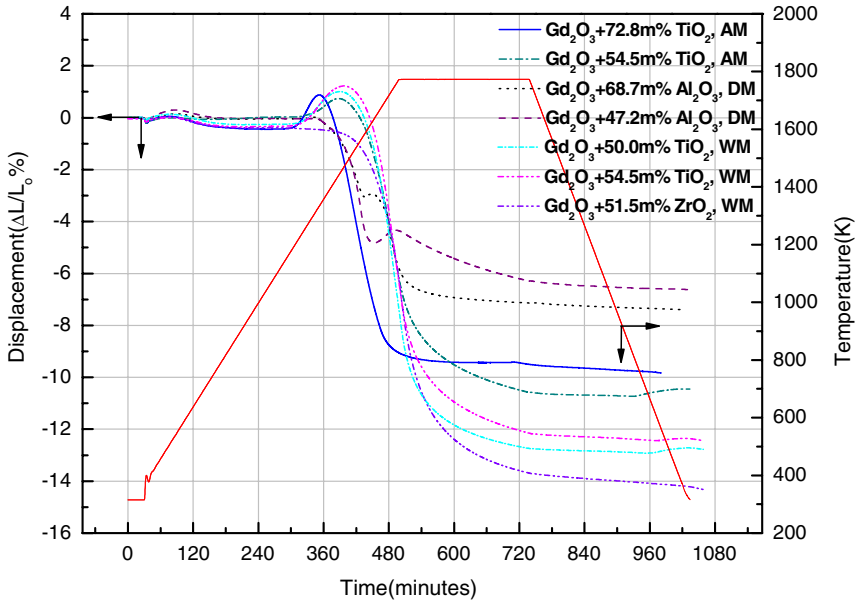

Fig. 2. Densification curves of Gd_2O_3 + diluent (diluent = TiO_2, ZrO_2 or Al_2O_3) during heat cycle.

had proceeded from 3% to 5%. The densification process of the $Gd_2O_3 + Al_2O_3$ was at the beginning even at the set temperature of 1773 K and the total shrinkage was far less than those for the other pellets at the same heat cycle. It is considered that the Gd_2O_3+ Al_2O_3 sinters at a considerably higher temperature in comparison with the other pellets.

On the basis of the densification behaviors of the green pellets, a sintering program for each pellet was determined by considering the mixing compositions and the milling methods. Several batches of the $Gd_xM_yO_z$ pellets were fabricated for an analysis of their thermal properties and an irradiation test as shown in Table 1. The chemical compositions of the GT2d and GT4 pellets, which were prepared for the irradiation test, were estimated by using ICPMS (inductively coupled plasma mass spectroscopy). The weight percents of Gd and Ti were 72.6 and 12.5 in the GT2d, and, 38.7 and 31.9 in the GT4, respectively.

Some typical microstructures and XRD patterns of the $Gd_xM_yO_z$ pellets are shown in Figs. 3 and 4, respectively. There are two binary compounds in the $Gd_2O_3 + TiO_2$ system with the mixing ratio of Gd_2O_3:TiO_2 equal to 1:1 and 1:2, respectively, in accordance with the equilibrium phase diagram [12]. These compounds have low forms of L1:1 and 1:2 which transform to high forms of H1:1 and 1:2 above 1985 K. Fig. 3(a) is the microstructure of the GT1w pellet which has a L1:1 phase. The L1:1 phase only exists on the line of a phase boundary with a molar ratio of Gd_2O_3:TiO_2 = 1:1 stoichiometric composition. XRD analysis of Fig. 4 shows that the GT1 w pellet consists of a single phase of L1:1 with an orthorhombic structure. The L1:1 phase has unit cell parameters of $a = 1.04788$ nm, $b = 1.132\ 8$ nm, and $c = 0.37547$ nm [5]. Fig. 3(b) shows the microstructure of the GT2w pellet which was studded with grains, relatively large and small ones. Phase structure of the GT2w pellet was a mixture of the L1:1 and 1:2 phases as shown in Fig. 4. GT3 pellet consists of a single 1:2 phase as shown in Fig. 4. The 1:2 phase has a cubic pyrochlore structure of which the unit cell parameter is $a = 1.01852$ nm. When compared with the microstructures of GT1w and GT2w, the grain size was in a reverse order with regard to the TiO_2 content. Fig. 3(c) shows the microstructure of the GT4 pellet. This pellet was sintered at 1723 K, which is a lower temperature than that for the other pellets, because of the eutectic reaction between a pyrochlore and a rutile (TiO_2). The XRD result shows that the GT4 pellet is a mixture of the 1:2 phase and a rutile phase. The rutile phases with a fine grain size were homogeneously distributed with normal 1:2 grains in the microstructure of GT4. The microstructure of the GZ pellet is shown in Fig. 3(d). The GZ pellet might have a single fluorite-type phase according to its composition and phase diagram [10,13]. However, XRD peaks of GZ could not be analyzed because there was no data that could match with the peaks. Fig. 4 shows that the XRD peaks of the GA matched with the data for $GdAlO_3$ exactly. It is clear that the Gd_2O_3 + 47.2 mol.% Al_2O_3 forms a solid solution, which represents a $GdAlO_3$ phase after a sintering. The $GdAlO_3$ phase has an orthorhombic structure with the lattice parameters of $a = 0.5250$ nm, $b = 0.5302$ nm and $c = 0.7447$ nm.

3.2. Thermal properties of the $Gd_xM_yO_z$ pellets

Fig. 5 shows the thermal expansion of the $Gd_xM_yO_z$ pellets from room temperature to 1773 K. The thermal expansion of the GT1w pellet with an orthorhombic L1:1 phase showed the lowest values, when compared with those of the other pellets. Whereas the GT3 pellet with a cubic pyrochlore phase showed the highest thermal expansion.

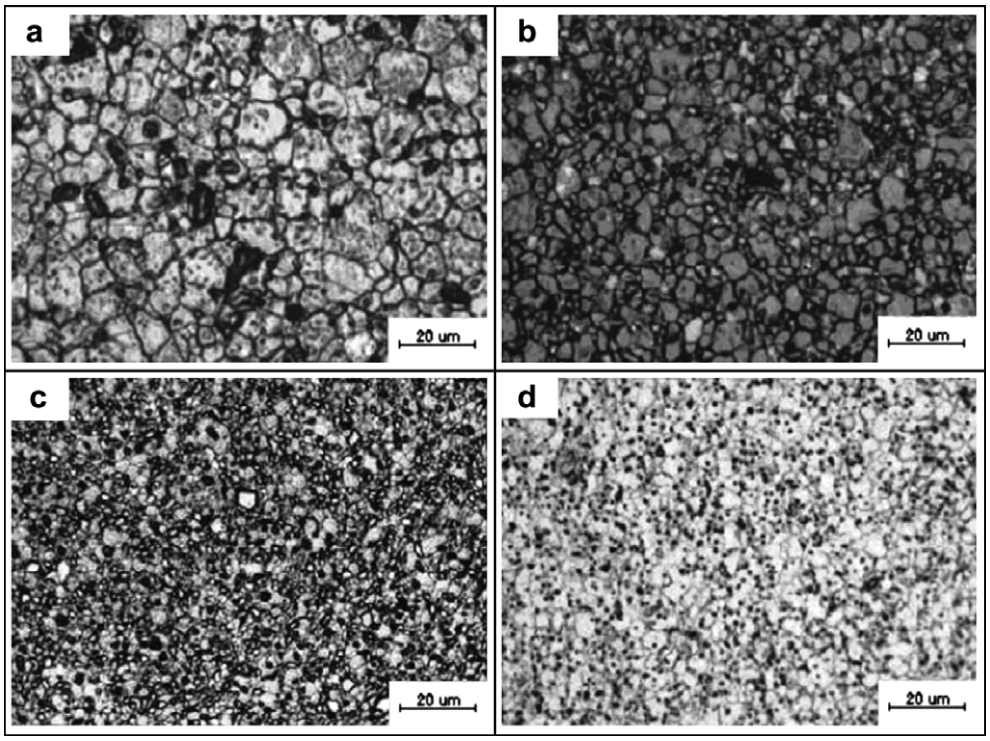

Fig. 3. Microstructures of $Gd_xM_yO_z$ pellet: (a) GT1w, (b) GT2w, (c) GT4, and (d) GZ.

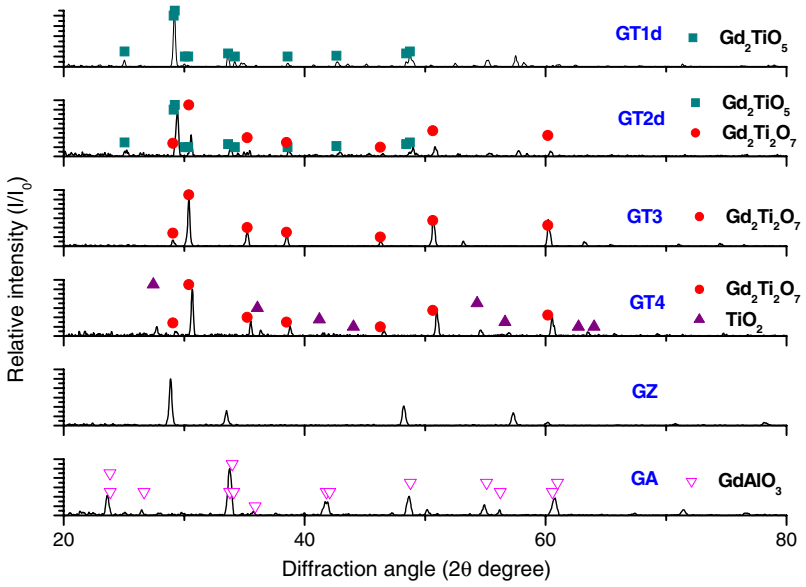

Fig. 4. XRD patterns of $Gd_xM_yO_z$ pellet.

GT2w pellet, which had the L1:1 and 1:2 phases showed a medium thermal expansion between GT1w and GT3. Thermal expansion coefficients of GT1w and GT3 calculated by a linear regression were 4.8×10^{-6}/K and 1.0×10^{-5}/K, respectively. The expansion curves of the GZ and GA pellets were nearly overlapped between room temperature and around 1300 K. The expansion coefficient in the overlapped range was 9.7×10^{-6}/K. Two break points existed on the expansion curve of GZ at around 1370 K and 1470 K. The breakpoints in the thermal expansion curves could be a sign of a phase transformation. There are some disputes in terms of the phase structures between a pyrochlore and a fluorite-type $Gd_2Zr_2O_7$ compound. A defective fluorite structure gradually orders itself, forming a pyrochlore superstructure

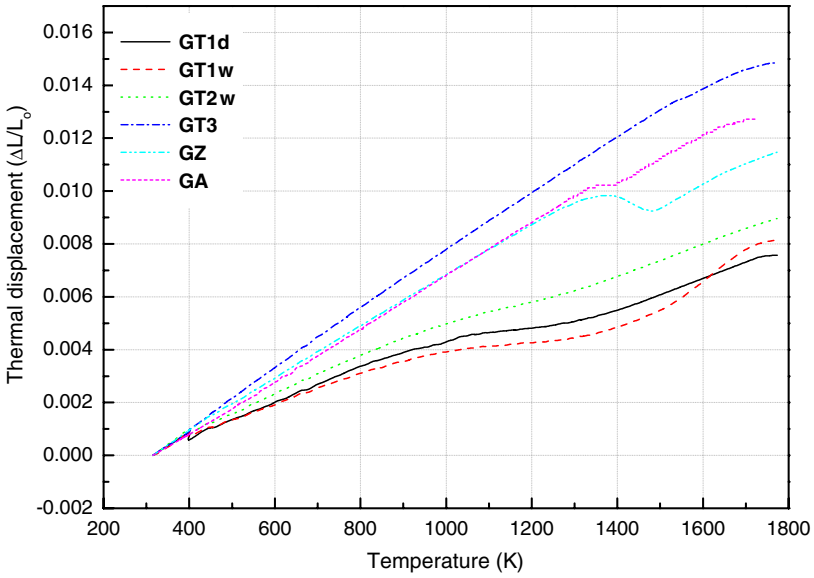

Fig. 5. Thermal displacement versus temperature for $Gd_xM_yO_z$.

[9,10]. The lattice parameter of 1.0523 nm for the pyrochlore structure is about twice as large as that of 0.5102 nm for the fluorite structure. Both phases could be formed in the $Gd_2O_3 + ZrO_2$ system for $0.18 \leqslant x \leqslant 0.62$ with $x =$ Gd content [10]. It is known that the $Gd_2Ti_2O_7$ also undergoes an order–disorder transition at about 1823 K, by transforming from a pyrochlore to a fluorite structure [9,12]. A phase structure which maintains a stable geometry with a temperature change is an advantage as a BP absorber. The GT1w with a single L1:1 phase is a recommendable material in terms of a thermal expansion.

A BP absorber generates a significant amount of heat itself by a reaction with a neutron under irradiation. The generated heat has to be transferred through the BP pellet to a coolant under a temperature gradient, so the thermal conductivities of the $Gd_xM_yO_z$ pellets are important for an application as BP absorbers. The thermal conductivity (K_{th}), the proportionality factor being a material constant, was derived from the measured data of thermal diffusivity (α_{th}), specific heat capacity (c_p) and density (ρ).

The thermal diffusivities of $Gd_xM_yO_z$ are shown in Fig. 6. All the measured data decreases with a temperature increase in the range of 300–800 K and then flattens off. The diffusivities of GA and GT4 were higher than those of the other samples. The diffusivity value was in the order of GT4, GT2d, GT1d, so they decreased with an increasing

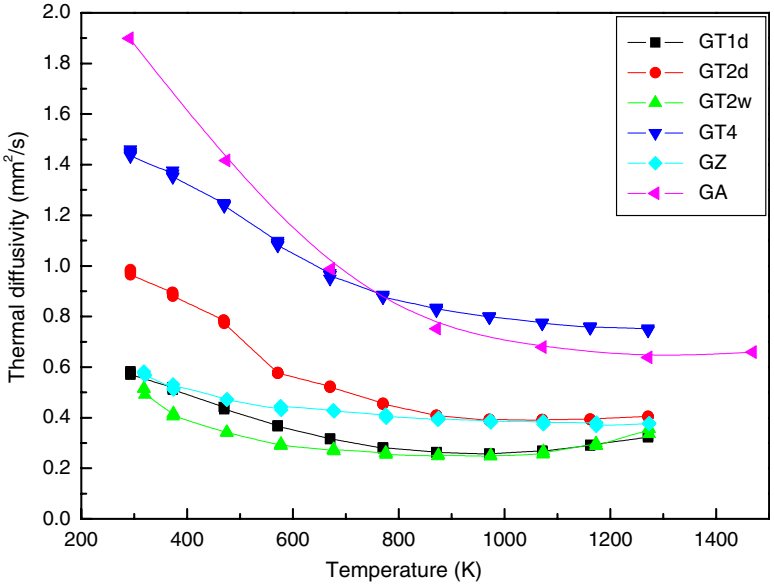

Fig. 6. Thermal diffusivities of $Gd_xM_yO_z$.

gadolinium concentration in the $Gd_xTi_yO_z$ samples. The diffusivity of GZ was similar to that of GT1d at room temperature and nearly constant with temperature above 600 K.

Fig. 7 shows the specific heat capacities which are the measures of the energy required to raise the temperature of the $Gd_xM_yO_z$. The measured heat capacities usually increased with the temperature except that of GT4. The heat capacity increased with the Ti content in the $Gd_xTi_yO_z$, which was the same as the case of the thermal diffusivity. The heat capacity of GT1d was a little lower than that of GT2d, but very similar to each other, since there was a small difference in the Ti content between them, $Gd_2O_3 + 50$ mol.% TiO_2 for GT1d and $Gd_2O_3 + 54.5$ mol.% for GT2d. The heat capacity of GZ was about the same as that of GT1d at room temperature but it increased more rapidly with temperature. The heat capacity of GA was lower than that of GT4 below 800 K, but it was reversed above 800 K because of its upward tendency with the temperature, like that of GZ.

Thermal conductivities of $Gd_xM_yO_z$ were derived from the expression $K_{th} = \alpha_{th} c_p \rho$. The derived thermal conductivities are shown in Fig. 8. As expected from the results of the thermal diffusivity and the heat capacity measurements, the thermal conductivities of $Gd_xTi_yO_z$ decreased in the order of GT4, GT2d, and then GT1d, with an

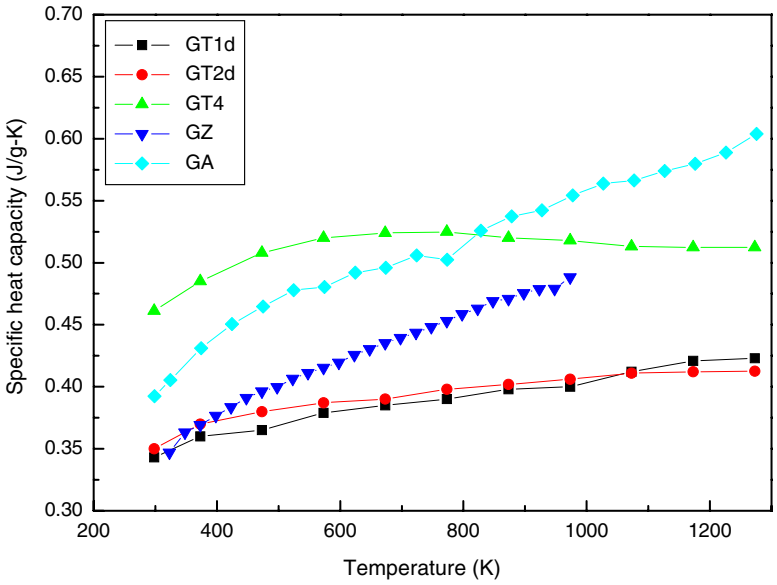

Fig. 7. Specific heat capacities of $Gd_xM_yO_z$.

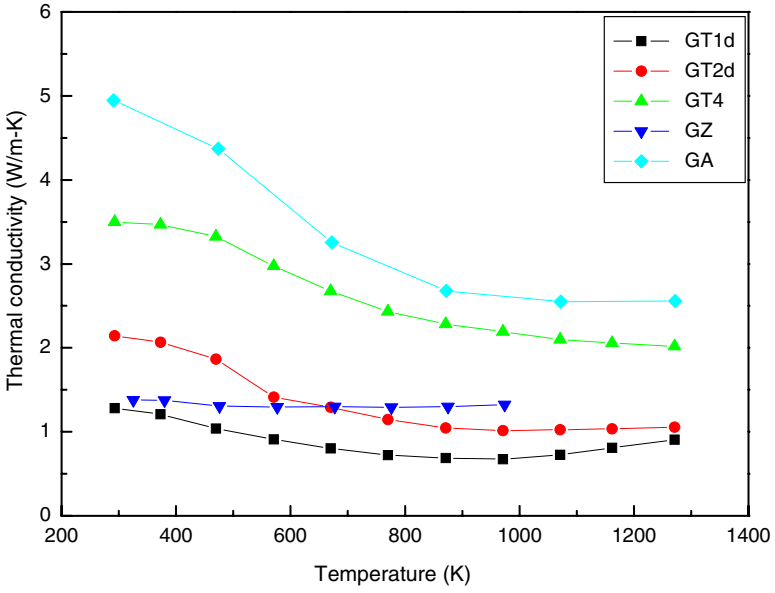

Fig. 8. Thermal conductivities of $Gd_xM_yO_z$.

increasing gadolinium concentration. The thermal conductivity of GA was higher than the other solid solutions, but it decreased rapidly with the temperature, when compared with the others. The solid solution of $Gd_xAl_yO_z$ had the best thermal conductivity but its high thermal expansion is a negative aspect for a BP pellet. The thermal conductivity of GZ was similar to that of GT1d at around 300 K, but higher than those of GT1d and GT2d above 700K because it is relatively constant with the temperature.

On the assumption that the sintered density of the $Gd_xTi_yO_z$ pellets has 95% of the theoretical density, the gadolinium concentration of a sample, gadolinium weight in unit volume of the $Gd_xTi_yO_z$ pellet, is as follows: 4.6 g/cm^3 for GT1d, 4.2 g/cm^3 for GT2d, 2.0 g/cm^3 for GT4. The gadolinium concentration is an important value, when designing a nuclear fuel assembly as well as a reactor core. Several types of BP rods are necessary to compensate for the excess reactivity and to control the power distribution homogeneously in a reactor. First of all, the type of BP rod must be classified according to the gadolinium concentration of the BP pellets contained in it.

Both the thermal expansion and the thermal conductivity of the $Gd_xTi_yO_z$ pellet were affected by the gadolinium concentration as shown in Figs. 5 and 8. The BP absorber undergoes all sorts of hardships with a nuclear fuel during irradiation. A high thermal conductivity with a low thermal expansion is desirable for the BP pellet. When considering both the thermal expansion and the thermal conductivity requirements for a BP absorber, GT2 and GT4 are recommended.

3.3. Irradiation test and PIE

Four pellets of GT2d with a gadolinium concentration of 4.2 g/cm^3 and four pellets of GT4 with that of 2.0 g/cm^3 were irradiated for 254 EFPD, and the accumulated neutron fluence was 5.1×10^{20} neutrons/cm^2. This test was aimed at investigating the in-pile performance of $Gd_xTi_yO_z$ as a (n,γ) burnable absorber.

Post-irradiation examinations were conducted on the fabricated capsule. Fig. 9 shows the visual examinations performed by using a hot cell periscope and an in-cell video camera. GT2d pellets were easily unloaded by tilting and tapping the sample tube. All the GT2d pellets had maintained their geometrical integrity after the irradiation test. The initial radial gap between the sample tube and the pellet was 50 μm, but the GT4 pellets were jammed by swelling during irradiation. Two pellets of GT4 were cracked during the process of a forceful extraction from the sample tube and the other two pellets remained in the tube.

The thermal expansion coefficient of the pyrochlore phase was higher than that of the others as shown in Fig. 5. It was anticipated that the thermal expansion of GT4 was greater than that of GT2d because GT4 is a mixture of the pyrochlore and rutile phases.

Macroscopic swelling of the curium doped $Gd_2Ti_2O_7$ has been observed as a function of the cumulative alpha decay dose [7]. The XRD results of the $Gd_2Ti_2O_7$ showed a general decrease in its relative XRD intensities and an amorphous state was reached at $1.7–1.9 \times 10^{25}$ alpha decays/m^3. Recrystallization of the amorphous phase led directly to an initial pyrochlore structure, beginning at about 973K and reaching a full recovery at 1123 K [7]. Under an irradiation of the GT2d and GT4 pellets in the HANARO reactor, the estimated center temperature was 1423 K and 1773 K with a radial power depression and a uniform power distribution, respectively [14]. Therefore, the initial structures of the GT2d and GT4 pellets were maintained by thermal recovery under irradiation.

The GT4 pellets could have come in contact with the inner wall of the sample tube by thermal expansion and irradiation swelling in the reactor so that they became jammed by cracking or chipping around the pellet edges. Some cracks and chips were observed in the radial section of an irradiated GT4 pellet as shown in Fig. 10. However, the GT2d pellets did not contain any micro-cracks, and they maintained their integrity intact after irradiation.

Dimensions of the un-irradiated GT2d pellets were compared with those of the irradiated pellets in Table 2. Calibration was done before the measurements, but some measurement errors can be induced because the measuring conditions and tools are different between the routine laboratory and the hot cell. According to the measured diameters in Table 2, two pellets were swollen in the radial direction, but the other two pellets were shrunk a little after irradiation. The in-reactor swelling of the GT2d pellets

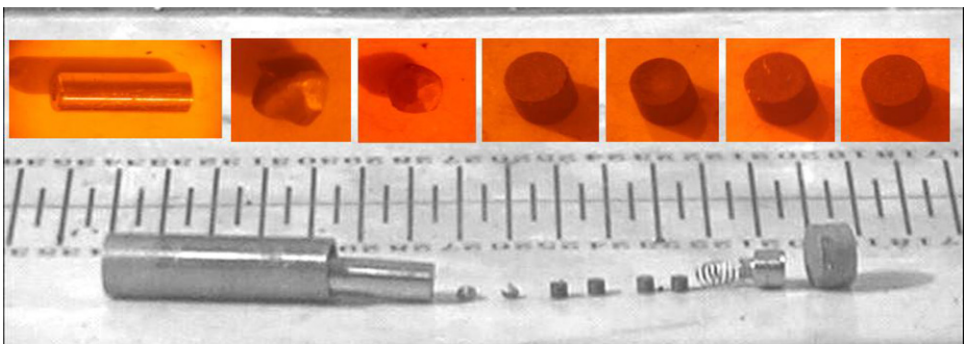

Fig. 9. Visual inspection of the GT2d and GT4 pellets after the irradiation test.

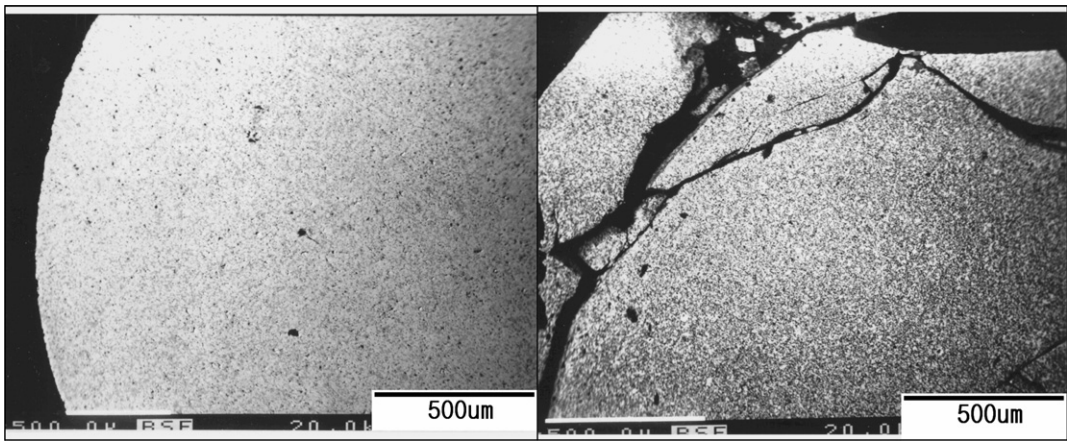

Fig. 10. Macroscopic views of the irradiated GT2d and GT4 pellets.

Table 2
Comparison of the dimensions for the un-irradiated GT2d pellets with those for the irradiated pellets

Sample ID	Before irradiation			After irradiation	
	Height (mm)	Diameter (mm)	Density (g/cm^3)	Height (mm)	Diameter (mm)
GT2d-5	3.084	3.472	6.22	3.275	3.500
GT2d-6	3.050	3.494	6.21	3.090	3.480
GT2d-7	3.098	3.497	6.27	3.135	3.500
GT2d-8	3.064	3.486	6.28	3.060	3.480

could have resulted from the presence of decay products and/or a displacement caused by a thermo-mechanical stress.

4. Conclusions

The different pellets of $Gd_xM_yO_z$ were investigated in order to develop a proper burnable poison material. The sinterability test showed that the shrinkages of $Gd_2O_3 +$ x mol.% TiO_2 were decreased with x and the sintering temperatures need to increase with x to obtain homogeneous solid solutions. The densification process of $Gd_2O_3 + ZrO_2$ was similar to that of $Gd_2O_3 + TiO_2$, but a breakpoint was not observed in the shrinkage curve.

The green pellets of the powder mixtures began to change into solid solutions after the sintering process; single L1:1 with an orthorhombic structure for $Gd_2O_3 +$ 50.0 mol.% TiO_2, L1:1 + pyrochlore for $Gd_2O_3 + 54.5$ mol.% TiO_2, pyrochlore + rutile for $Gd_2O_3 + 84.2$ mol.% TiO_2 and a single $GdAlO_3$ phase with an orthorhombic structure of $a = 0.5250$ nm, $b = 0.5302$ nm and $c =$ 0.7447 nm for $Gd_2O_3 + 47.2$ mol.% Al_2O_3.

L1:1 phase had the lowest thermal expansion, otherwise the pyrochlore phase had the highest value, when compared with those of the other phases. The thermal expansions of the GZ and GA were nearly the same between room temperature and around 1300 K, and the expansion coefficient was 9.7×10^{-6}/K.

The measured values of the thermal properties decreased with an increasing gadolinium concentration in the $Gd_xTi_yO_z$ samples. The thermal conductivity of $Gd_xAl_yO_z$ was higher than that of the other solid solutions, whereas $Gd_xZr_yO_z$ showed a relatively low but constant thermal conductivity with increasing temperature.

When considering both the thermal expansion and the thermal conductivity requirements for a BP absorber, GT2 and GT4 are recommended and consequently they were in-pile tested in the HANARO. It was observed that the GT2d pellets with a low thermal expansion property maintained their geometrical integrity and that they were easily extracted from the sample tube. On the contrary, the GT4 pellets were jammed within the sample tube, since they came in contact with the inner wall of the sample tube due to thermal expansion and irradiation swelling in the reactor.

Acknowledgements

The authors would like to thank many staffs working in HANARO and IMEF for nuclear physics calculation, irradiation test and PIE. This work was supported by the Ministry of Science and Technology (MOST) of the Republic of Korea under the nuclear R&D Project.

References

[1] Hugo van Dam, Ann. Nucl. Energ. 27 (2000) 63.
[2] J. Porta, S. Baldi, J.P. Chauvin, Ph. Fougeras, Prog. Nucl. Energ. 38 (2001) 355.
[3] Marielle Asou, Jacques Porta, Nucl. Eng. Des. 168 (1997) 261.
[4] V.D. Risovany, E.E. Varlashova, D.N. Suslov, J. Nucl. Mater. 281 (2000) 84.

[5] G. Panneerselvam, R. Venkata Krishnan, M.P. Antony, K. Nagarajan, T. Vasudevan, P.R. Vasudeva Rao, J. Nucl. Mater. 327 (2004) 220.
[6] H.S. Kim et al., J. Korean Cer. Soc. 39 (11) (2002) 1108.
[7] W.J. Weber, J.W. Wald, Hj. Matzke, J. Nucl. Mater. 138 (1986) 196.
[8] W.L. Gong, W. Lutze, R.C. Ewing, J. Nucl. Mater. 277 (2000) 239.
[9] A.J. Feighery, J.T.S. Irvine, C. Zheng, J. Solid State Chem. 160 (2001) 302.
[10] Junhu Wang, Akio Nakamura, Masuo Takeda, Solid State Ionics 164 (2003) 185.
[11] Y.W. Lee, H.S. Kim, S.H. Kim, C.Y. Joung, S.H. Na, G. Ledergerber, P. Heimgartner, M. Pouchon, M. Burghartz, J. Nucl. Mater. 274 (1999) 7.
[12] J.L. Waring, S.J. Schneide, J. Res. Nat. Bur. Stand. A 69 (3) (1965) 257.
[13] Monique Perez y Jorba, Ann. Chim. Paris 7 (1962) 509.
[14] B.H. Lee, H.S. Kim, J.M. Park, J.S. Cheon, J.Y. Oh, Y.H. Koo, J.S. Yim, D.S. Sohn, in: Proceedings of ICAPP'05, Seoul, Korea, May 15–19, 2005, paper 5311.